Bratina, S., Saje, M., Planinc. I. 2007. The effects of different strain contributions on the response of RC beams in fire. *Engineering Structures* 29,3: 418-430. DOI: 10.1016/j.engstruct.2006.05.008.

The effects of different strain contributions on the response of the RC beams in fire

Sebastjan Bratina, Miran Saje[1] and Igor Planinc

University of Ljubljana, Faculty of Civil and Geodetic Engineering
Jamova 2, SI-1115 Ljubljana, Slovenia

Abstract

A two-step formulation, consisting of separate thermal and mechanical analyses, is presented for the thermo-mechanical analysis of reinforced concrete planar frames subject to fire conditions. The heating and the cooling phases are considered. Standard planar, four-node quadrilater finite elements are employed in the non-linear time-dependent thermal analysis of cross-sections, while the recently proposed strain-based planar beam finite elements are used in the non-linear mechanical analysis of the frame [Bratina S, Saje M, Planinc I. On materially and geometrically non-linear analysis of reinforced concrete planar frames. International Journal of Solids and Structures 2004;41:7181–7207]. The formulation includes both exact geometric and material non-linearities, and considers the temperature dependence of thermal and material parameters, the plastic, creep and thermal strains in concrete and steel, the transient strain in concrete, and the strain localization as a consequence of softening of material at high temperatures. A so called 'constant strain element' is introduced to resolve numerically the loss of uniqueness of strain measures at the point of localization. The formulation is validated by comparing some of the present numerically predicted results with the data, measured in experiments. Although the present model is essentially 1D stress-strain model, and is thus simple in terms of the number of degrees of freedom used and ignores transfer of water in concrete during heating, the comparisons with the measured data are found to be satisfactory. In particular, the agreement of the fire resistance times and critical deflections between the predicted and the experimental values was found very satisfactory. In contrast, a disagreement was found in distributions of temperature over the beam cross-sections. The results make it possible to draw several conclusions concerning behaviour of structures in fire. In particular, it is established that the consideration of creep and transient strains in concrete has little effect on the fire resistance time of statically determinate beams under bending or unconstrained centrically loaded columns; their effect on displacements is, however, remarkable.

Keywords: reinforced concrete, creep, thermal strain, transient strain, fire resistance, strain-based finite element method.

[1]Corresponding author. Phone.: +386 1 4768 613; fax: +386 1 4768 629.

E-mail address: msaje@fgg.uni-lj.si (M. Saje)

1 Introduction

Fire resistance presents an important aspect of safety of structures. It is well known that the temperature increase in fire conditions decreases load-carrying capacity of concrete, and increases its deformability. Due to structural and chemical changes in material caused by the elevated temperature, due to the internal stresses enforced by the temperature gradient, and due to high pore pressures caused by the evaporation of pore water, internal microcracks or damages appear in concrete. Further on, at an elevated temperature, the decomposition process of the cement stone in concrete begins, which is the consequence of the dehydration of the cement binder. Physical-chemical changes appear also in the stoneware, which leads to the decomposition of aggregate grains. For this reason the decrease of compressive strength of concrete at an elevated temperature depends also on the type of aggregate used. The elastic and shear moduli of concrete decrease nearly linearly with the increase of temperature [8], in contrast to the thermal extension coefficient of concrete, which increases non-linearly [26]. Due to stresses in concrete caused by the temperature gradient, due to the increase of pore pressures [11, 19], and due to the fact that the thermal extension coefficient of steel reinforcement increases with temperature much faster than that of concrete, a concrete splitting may also appear.

The magnitude of concrete creep at elevated temperatures is much bigger than at room temperature. Cruz [9] measured the creep of concrete under a constant load and several different stabilized temperatures up to 650°C and Anderberg *et al.* [1] up to 790°C. They found out that temperatures only above 400°C are somewhat influential. In contrast, the effect of creep of a steel reinforcement onto stress and strain state in reinforced concrete frames is remarkable when temperature in reinforcement bars exceeds 400°C [41].

A particularity of concrete is the so called transient strain. This has been found to have an important effect on the mechanical behaviour of concrete during the first heating [1, 29, 32]. It is irecoverable and emerges as the result of the physico-chemical changes that take place only under the first heating. The transient strain aims to represent the inelastic deformations due to moisture effects such as the difusion and the evaporation [20] and mismatch between thermal deformations of aggregate and mortar [31, 38]. Formally, it may be defined as that part of the total strain obtained in stressed concrete under heating, which cannot be accounted for otherwise (for further details, see [1, 32]).

Shrinkage of concrete becomes somewhat more intensive at elevated temperatures, yet the related strains are small compared to overall strains and can be disregarded in the analysis [16, 36]. In contrast, the bond strength between concrete and steel may decrease substantially with increasing temperature [31, 35]. Yet the decrease of the bond strength and the related increased bond slip seem to affect the bearing capacity and its ductility only when the structure is made from pre-stressed concrete [31].

Spalling of fire-exposed concrete is another important phenomenon, in particular, if concrete is densified by particles smaller than the cement grains such as micro silica, and if the moisture content

is more than 3 % by weight. If the moisture content in traditional concrete is between 3 and 4 %, the risk of spalling is small [15, 31]. Spalling may either progress slowly ('progressive spalling') as a consequence of deteriorating strength of concrete, steel and bonding, or appears instantaneously in a form of explosion ('explosive spalling'). While the effect of the former is only minor, the effect of the explosive spalling can be disastrous. The explosive spalling is now well understood, being the result of a combined effect of high pore pressure and constrained deformations between agreggate and cement stone [19, 37, 39, 40]. Yet, and as pointed out by Hertz [15], the further research is needed in order to develop a coherent theory and to establish the design methods for engineers.

It is clear that high temperature and its rapid variation in fire conditions trigger a number of complex and interrelated physical, mechanical and thermo-hydral phenomena in a reinforced concrete structure [22]. Comprehensive 3D numerical modelling is hence both theoretically and numerically a very difficult task. These analyses are typically used in the comprehensive study of behaviour of unique engineering structures, such as atomic power plants or high-way tunnels [18, 27], where the fire response is modelled as a fully coupled thermo-hydro-mechanical problem [13, 28, 38]. A much less sophisticated are the formulations, where the mechanical and the thermo-hydral processes are uncoupled, which makes it possible to study the fire response of a structure in two separate steps. In the first step, the heat and mass transfer during fire is determined, which is then, in the second step, employed as the time-dependent thermal load in the mechanical analysis [3, 10]. This is a reasonable assumption, because the contribution of the mechanical work to the change of temperature is small compared to the heat input during fire, and because water is much more incompressible than concrete [3]. For reinforced concrete frame structures made from traditional concretes, where the explosive spalling is uncommon, we believe that the mathematical model employed in the design methods for engineers can further be simplified, i.e., the water and vapour transfer and phase changes in water can be neglected (as suggested in Eurocode 2 [10]) or indirectly accounted for by an artificially increased specific heat of concrete [10], or we do consider these effects, yet in an uncoupled sense [24]. The simplified mechanical model of the reinforced concrete framed structure is typically a framework of 1D beam elements, see [4, 7, 24, 25].

In the present paper we follow the above simplifying logic. The novelty of our approach is the introduction of the original strain-based planar beam finite element [4]. There are several advantages of this new finite element: (i) outstanding accuracy of both displacements and internal forces; (ii) insensitivity to locking; (iii) numerical robustness; (iv) good radius of attraction in Newton's iteration. Furthermore, it enables to introduce the strain-softening driven localization into the formulation in a natural way [4, 33]. This is an important issue, since the collapse of reinforced concrete structures in fire is typically a consequence of a series of strain localizations in the structure [3] due to the concrete softening in its post-peak stress-strain behaviour.

An aspect of utmost importance of the present fire analysis is that such a numerical analysis makes it possible to quantify the particular contributions of plastic, thermal, creep and transient strains to the total deformation of a structure. In fact, the main objective of the present paper is to

show and discuss the effect of particular types of strains on behaviour, collapse load, resistance time and ductility of a reinforced concrete beam subject to fire.

The present computational model and the related computer program for the non-linear analysis of the response of planar reinforced concrete frames simultaneously exposed to fire and external mechanical loads up to the failure have already been described to some extent in [4, 5, 6, 30]. That is why we here present only the details that are relevant to the present discussion.

2 Mechanical properties of concrete and reinforcing steel

In a time increment, Δt, the geometric (or total) extensional strain increment, ΔD, of a generic material fibre of a beam is assumed to be the sum of increments of elastic, ΔD_{e}, plastic, ΔD_{p}, thermal, ΔD_{th}, creep, ΔD_{cr}, and transient strain increment, ΔD_{tr}, the latter being non-zero only in concrete. These increments of strain are assumed to be given functions of the stress and temperature, as described in the sequel.

2.1 Mechanical strain

The sum of elastic and plastic parts of the strain increment will be termed the mechanical strain increment, $\Delta D_\sigma = \Delta D_{\mathrm{e}} + \Delta D_{\mathrm{p}} = \Delta D - \Delta D_{\mathrm{th}} - \Delta D_{\mathrm{cr}} - \Delta D_{\mathrm{tr}}$. We assume that the relationship between the mechanical strains and the longitudinal normal stress, σ, is given by the constitutive law $\sigma = \mathcal{F}(D_\sigma, T)$, where $\mathcal{F}$ is a functional pertinent to the chosen material. In the present fire analysis, we use the temperature dependent constitutive laws of concrete and reinforcing steel as suggested in Eurocode 2 [10]. An isotropic strain-hardening model is assumed in the loading–unloading cycles.

2.2 Thermal strain

The thermal strain in concrete and steel, $D_{\mathrm{th,c}}$ and $D_{\mathrm{th,s}}$, is assumed to be a function of the current temperature, T, and is given by the generic relation $D_{\mathrm{th}} = \tau(T)$. The approximation of functional τ for concrete and steel as defined in Eurocode 2 [10] is adopted here.

2.3 Concrete creep strain

The concrete creep strain, $D_{\mathrm{cr,c}}$, is assumed to be a function of the current stress, time and temperature. We employ the model proposed by Harmathy [14]. He assumes constant stress and temperature during experiment and proposes the law for the creep strain evolution in the form

$$D_{\mathrm{cr,c}} = \beta_1 \frac{\sigma_{\mathrm{c}}}{f_{\mathrm{cT}}} \sqrt{t}\, \mathrm{e}^{d(T-293)}\,. \tag{1}$$

Here t [s] marks the time and f_{cT} is strength of concrete at temperature T [K]. Empirical constants β_1 [$\mathrm{s}^{-1/2}$] and d [K^{-1}] have been determined by fitting the results of the creep tests of Cruz [9] ($\beta_1 = 6.28 \cdot 10^{-6}\,\mathrm{s}^{-1/2}$, $d = 2.658 \cdot 10^{-3}\,\mathrm{K}^{-1}$) using the method of least squares.

In practice, temperature in interval $[t^j,\, t^{j+1}]$ changes with time and likewise does the stress. In order to employ the constant-stress and constant-temperature law (1) for the situation in which stress and temperature change with time, we have applied the following algorithm [1]:

(i) prescribe time t^{j+1} and compute the time increment, $\Delta t^{j+1} = t^{j+1} - t^{j}$;

(ii) compute a relative time, t^{j}_{m}, which, at constant stress $\sigma^{j+1}_{\mathrm{c}}$ and constant temperature T^{j+1}, would result in the given creep strain $D^{j}_{\mathrm{cr,c}}$ at t^{j}. This requirement yields

$$t^{j}_{\mathrm{m}} = \left(\frac{D^{j}_{\mathrm{cr,c}}}{\beta_1 \, \frac{\sigma^{j+1}_{\mathrm{c}}}{f^{j+1}_{\mathrm{cT}}} \, \mathrm{e}^{d(T^{j+1}-293)}} \right)^{2};$$

(iii) compute the relative time $t^{j+1}_{\mathrm{m}} = t^{j}_{\mathrm{m}} + \Delta t^{j}$;

(iv) in formula (1), substitute t with t^{j+1}_{m}, T with T^{j+1}, σ_{c} with $\sigma^{j+1}_{\mathrm{c}}$, and f_{cT} with f^{j+1}_{cT}, and compute the creep strain $D^{j+1}_{\mathrm{cr,c}}$.

Fig. 1 shows the comparisons between the experimental and analytical results for creep strain using Eq. (1) at various constant temperatures in the range from 24°C to 649°C.

A different model was suggested by Kang *et al.* [20], in which the creep strain depends on two parameters of concrete, i.e. the creep activation energy and the gass constant along with temperature and time.

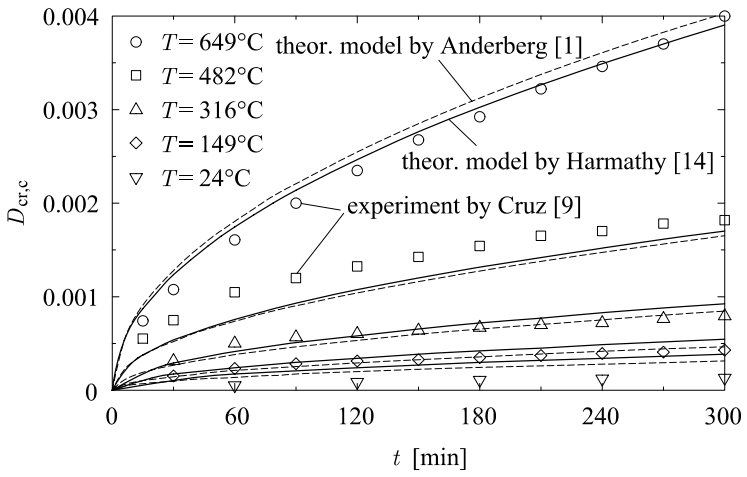

Fig. 1 The variations of creep strain with time according to the models proposed by Harmathy [14] and Anderberg *et al.* [1] and the experimental data by Cruz [9].

We wish to emphasize that the majority of numerical formulations of the fire analysis of the reinforced concrete structures do not differentiate between the plastic and creep strains in concrete. They employ the combined plastic strain, which includes both the plastic and the creep strain parts. The stress in concrete is then taken to be a function of this combined strain [24, 25, 42]. Such a material model cannot account for the rates of temperature and creep strain properly, neither is able to divide the resulting combined plastic strain into the actual plastic and creep parts. The transient creep in concrete is usually ignored [42]. By contrast, the present formulation considers each of the physical strain parts separately, thus enabling an engineer to follow the time variation of each particular strain and to assess its contribution to the total strain. This holds true for both concrete

and steel materials.

2.4 Steel creep strain

There is a number of creep models available for steel at high temperatures. In our research we have employed the model proposed by Williams-Leir [41]. This model assumes that the creep strain is a function of the current stress and temperature in steel, and that its evolution in time is governed by the differential equation

$$\dot{D}_{\mathrm{cr,s}} = \mathrm{sgn}(\sigma_{\mathrm{s}})\; b_1 \coth^2(b_2|D_{\mathrm{cr,s}}|)\,. \tag{2}$$

Material parameters b_1 and b_2 are functions of stress and temperature in steel [41]. Even if we assume that σ_{s} and T are given functions of time, Eq. (2) is a complicated differential equation that needs to be integrated numerically. The present solution method substitutes the time derivative with the implicit differential quotient in time and the resulting algebraic equation is then solved iteratively by the Newton method.

2.5 Concrete transient strain

We adopt the transient strain model of Anderberg *et al.* [1, 31, 38], who assume

$$\Delta D_{\mathrm{tr,c}}^{j+1} = k_2\,\frac{\sigma_{\mathrm{c}}^{j+1}}{f_{\mathrm{c0}}}\,\Delta D_{\mathrm{th,c}}^{j+1} \qquad \text{for} \qquad T \le 550^o C, \tag{3}$$

$$\frac{\partial D_{\mathrm{tr,c}}}{\partial T} = 0.0001\frac{\sigma_{\mathrm{c}}^{j+1}}{f_{\mathrm{c0}}} \qquad \text{for} \qquad T > 550^o C. \tag{4}$$

Here $f_{\mathrm{c0}} > 0$ is strength of concrete at room temperature and $k_2 > 0$ is a dimensionless material constant whose value ranges from 1.8 to 2.35. Note that the transient strain is proportional to σ_{c} and thus has a sign that is opposite to the sign of $\Delta D_{\mathrm{th,c}}$ when concrete is stressed in compression.

Although the Anderberg model is often used [21, 26, 29], its suitability for the range of temperatures above 550°C may be questioned [1]. An alternative model for the transient strain of concrete, which combines the creep and the transient strain under the common name 'transient creep', has been proposed by Schneider [36] or recommended by Rilem [32].

2.6 Cooling phase

The appropriate treatment of the cooling phase is essential for the determination of the residual bearing capacity of the structure. Unfortunately, the measured data describing behaviour of concrete during the cooling phase are scarce and insufficient for reliable numerical analyses. That is why one is forced to introduce further assumptions. We assume that the stress–strain curve of concrete in a cooling stage, i.e. when temperature at material point starts decreasing, remains as it was at the instant of the outset of cooling. This is conservative, yet a rather realistic assumption, which is based on the fact that concrete strength deteriorates during heating. Following [1] we neglect the transient strain in concrete in the cooling phase. We treat the creep strain in the same way as in the heating phase, but note that there is no firm experimental evidence that either confirms or denies this

assumption. The thermal strains during cooling are assumed reversible and the same law is taken as during the temperature increase; as noted by Schneider [36], this may not hold for temperatures above 600°C and will need some further experimental research in future.

The response of steel bars (with regard to the stress–strain law, creep and temperature strains) during the cooling phase is assumed equal as in the heating phase.

3 Validation of the numerical model and parametric studies

3.1 Simply supported reinforced concrete beam with overhangs

Our first numerical example is a simply supported concrete beam with overhangs. This beam has been extensively tested by Lin *et al.* [26] and their results will be used to validate the present numerical model. In what follows three variants of this beam will be analysed and marked as B_1, B_3 and B_5 [26]. Geometric, material and loading data are given in Fig. 2 and in Table 1, where f_{c0} and f_{y0} denote the compressive strength of concrete and the ultimate strength of steel at room temperature, respectively. One may see from the table that beams B_1 and B_3 were exposed to the standard fire with only an increasing temperature as specified in the ASTM Designation [2], while beam B_5 was tested under the temperature exposure with the subsequent cooling phase (the SDHI-M fire [26]). During the tests the beams were loaded with six time-independent vertical forces P and force P_0 on the right overhang, which varies with time (see [26]). Note that the external dimensions of the cross-section of beams B_1, B_3 and B_5 and the areas of the steel reinforcement are equal, the only difference between beam B_3 and the remaining two ones being the thickness of the concrete cover, see Fig. 2 and Table 1.

Beam specimen [26]	B_1	B_3	B_5
concrete cover [mm]	38	57	38
fire curve	ASTM	ASTM	SDHI-M
test duration [min]	220	243	243
P_0 (at $t = 0$ min) [kN]	115.7	115.7	115.7
P_0 (at $t = 240$ min) [kN]	166.5	160.1	166.5

Table 1 Details of beam specimens B_1, B_3 and B_5.

3.1.1 Temperature distribution in the beam

As discussed in the introduction, the temperature distribution in the beam is assumed uncoupled from the mechanical analysis and can thus be obtained separately. The assumption is realistic, because no explosive spalling during the experiment was reported by Lin *et al.* [26], indicating

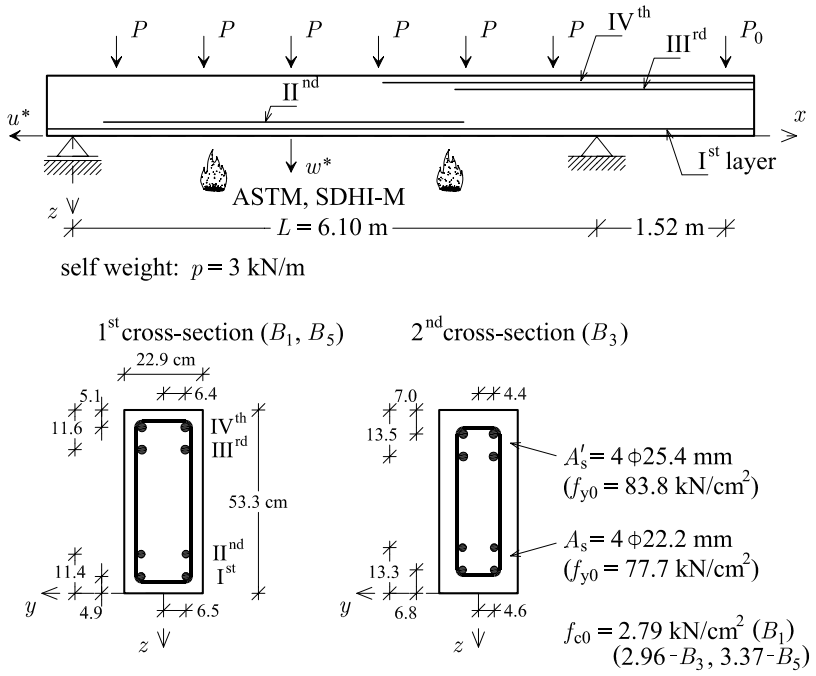

Fig. 2 A simply supported concrete beam with overhangs [26].

that there is no reason for the coupled analysis. Our further assumption is that the heat transfer in the longitudinal direction is much slower compared to the heat transfer over the cross-section and can hence be neglected. Therefore only the analysis of the heat transfer over a typical cross-section suffices. As area of steel reinforcement is small compared to area of concrete, its effect onto the temperature distribution over the concrete cross-section was neglected [10, 26]. `Pri tem pa smo upoštevali, da ima armatura enako temperaturo kot beton na mestu armature.` Due to symmetry of the cross-section only one half of the cross-section was modelled. The mesh with 672 four-node square finite elements [34] was used. The time step was 1 min. The thermal properties of concrete and steel used in the experiment are not given in [26] and had to be estimated. Somewhat modified thermal properties of concrete and steel were assumed in order to approximate in the best possible way the variation of temperature obtained in the experiment.

The heat transfer coefficient for the ASTM fire curve was assumed to be $\alpha_c = 8\,\mathrm{W/m^2K}$ for the bottom surface, and $\alpha_c = 30\,\mathrm{W/m^2K}$ for the lateral surfaces. For the SDHI-M fire curve, these parameters took values $10\,\mathrm{W/m^2K}$ and $20\,\mathrm{W/m^2K}$, respectively. The emissivity of the concrete surface in the ASTM fire load was assumed to be $\varepsilon_r = 0.1$ for the bottom surface and $\varepsilon_r = 1.0$ for the lateral surfaces; in the SDHI-M fires, these values were taken to be 0.15 and 0.3. The upper surface of the beam was not exposed to fire [26]. The conductivity of concrete (k) was chosen so that the calculated and the measured distributions of temperature over the cross-section agreed as much as possible (see Fig. 3). The values of density, ρ_c, and the specific heat of concrete, c_c, were taken from Eurocode 2 [10]. Note that the effect of steel reinforcement onto the temperature distribution over

the concrete cross-section was neglected.

Figs. 4 and 5 show the comparison of the predicted and the measured development of temperatures in steel bars in time. In these figures, the bottom steel bars are marked as Ist and IInd layer, while the top steel bars at the support are marked as IIIrd and IVth layer. The results differ somewhat, but the shapes of the calculated curves compare well with those of the experiments. The numerically predicted time variations of temperatures in the IIIrd and IVth layers are found to be nearly equal and therefore only one curve is plotted in Figs. 4 and 5.

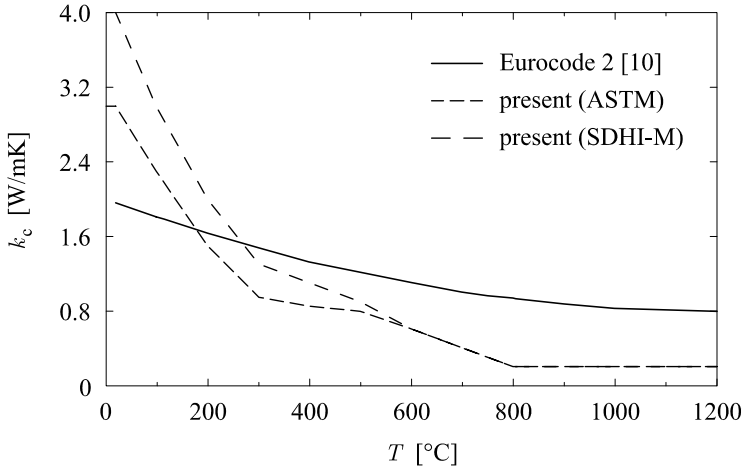

Fig. 3 Simply supported beam with overhangs [26]. The variation of conductivity k_c with temperature.

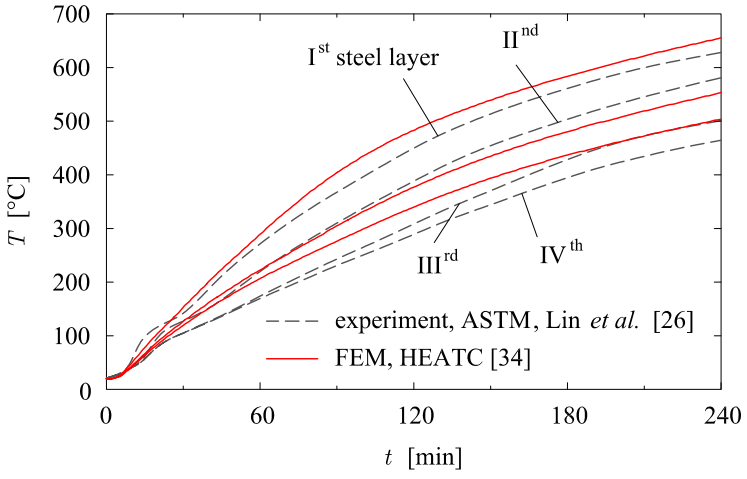

Fig. 4 Simply supported beam with overhangs [26]. The comparison between predicted and measured temperatures in steel layers for ASTM fire load.

Figs. 6 and 7 show the comparisons of the variations of the predicted and the measured temperatures in the cross-section along the vertical line $y = 7\,\mathrm{cm}$ for the ASTM and SDHI-M fire loads. It

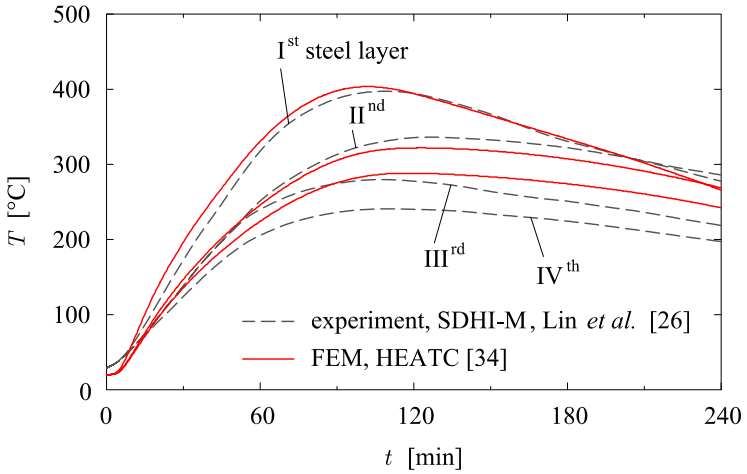

Fig. 5 Simply supported beam with overhangs [26]. The comparison between predicted and measured temperatures in steel layers for SDHI-M fire load.

is clear that the peak temperature values at the cross-section boundary $z = 53.3\,\text{cm}$ at the indicated times are not well reproduced by the numerical results; a somewhat better agreement seems to be found between the temperature gradients.

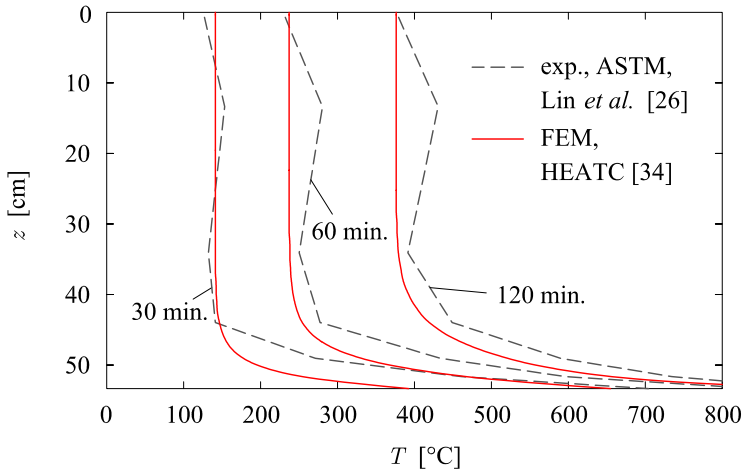

Fig. 6 Simply supported beam with overhangs [26]. Variations of predicted and measured temperatures in the cross-section along the vertical line $y = 7\,\text{cm}$ with time. ASTM fire load.

3.1.2 Mechanical response

The beam was modelled by ten standard strain-based finite elements, in which axial and bending strains were interpolated by Lagrangian polynomials of the fourth order, and, in addition, by two 'short' constant-strain finite elements, placed to the left side of the right support and to the left support of the beam. These short elements were used to capture the localization of deformations

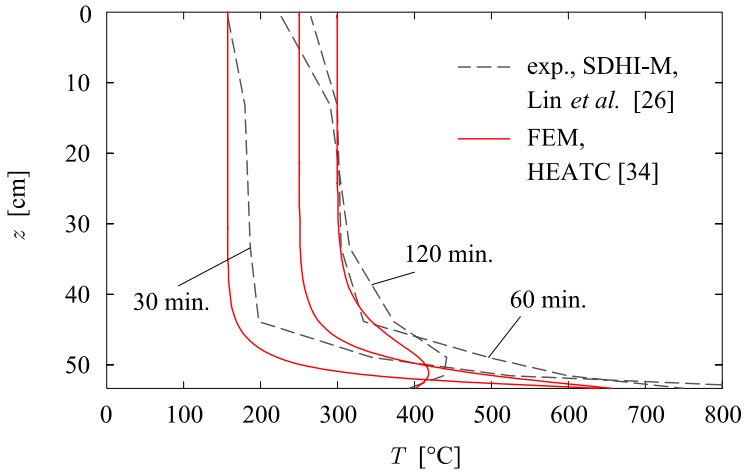

Fig. 7 Simply supported beam with overhangs [26]. Variations of predicted and measured temperatures in the cross-section along the vertical line $y = 7\,\text{cm}$ with time. SDHI-M fire load.

(for the detailed description of the short element, see [5]). The cross-sectional integration needed to determine the constitutive axial force, the constitutive bending moment and the cross-sectional constitutive tangent stiffness matrix was performed numerically. Note that due to the 2D distribution of temperature over the cross-section, the 2D integration is required (which is in contrast to structures which are not thermally loaded, where the 1D integration over the cross-sections suffices). We used the 3×3-point Gaussian integration with the total of 180 integration points over one half of the cross-section. The time step was 1 min at the beginning and 5 min after 10 min. The thermo-mechanical properties of concrete with calcareous aggregate and cold worked reinforcing steel were used.

One of the objectives of the present analysis was to assess the effect of various strain parts on the mechanical response of the beam. We performed four analyses, see Table 2.

Type of analysis	Strains considered
Case ***A***	D_{th}
Case ***B***	D_{th} and $D_{\text{cr,c}}$
Case ***C***	D_{th}, $D_{\text{cr,c}}$ and $D_{\text{tr,c}}$
Case ***D***	D_{th}, $D_{\text{cr,c}}$, $D_{\text{tr,c}}$ and $D_{\text{cr,s}}$

Table 2 Simply supported beam with overhangs [26]. The cases studied with the aim to estimate the partial effect of various strains on the mechanical response.

Stress–strain state in beam B_1. Most of the thermo-mechanical parameters of concrete were taken from Eurocode 2 [10]. They are: elastic modulus of concrete $E_{\text{c0}} = 3\,000\ \text{kN/cm}^2$; charac-

teristic strains of concrete: $D_{c10} = -2.5\,{}^{\circ}/_{\circ\circ}$ and $D_{cu0} = -20\,{}^{\circ}/_{\circ\circ}$; elastic modulus of steel $E_{s0} = 20\,000$ kN/cm^2; characteristic strains of steel: $D_{y1} = 20\,{}^{\circ}/_{\circ\circ}$, $D_{y2} = 50\,{}^{\circ}/_{\circ\circ}$ and $D_{yu} = 100\,{}^{\circ}/_{\circ\circ}$. Our objective is to estimate the partial effects of thermal strain, D_{th}, creep strain in concrete, $D_{cr,c}$, transient strain in concrete, $D_{tr,c}$, and viscous strain in steel, $D_{cr,s}$, on the response of the beam. Lin *et al.* [26] tested two specimens, marked B_{1a} and B_{1b}; the test conditions for the two geometrically equal specimens were assumed equal except that the strength of concrete in B_{1b} was found to be somewhat bigger (3.1 kN/cm^2 compared to 2.79 kN/cm^2 in specimen B_{1a}). The comparisons between various experimental and numerical values are for the instant $t = 200$ min presented in Table 3.

	experiment [26]		present			
	B_{1a}	B_{1b}	Case $\boldsymbol{A}$	Case $\boldsymbol{B}$	Case $\boldsymbol{C}^{\dagger}$	Case $\boldsymbol{D}^{\ddagger}$
w^* [cm]	12.4	14.6	8.31	8.66	10.16	12.43
u^* [cm]	6.2	7.5	5.16	5.12	4.99	5.22
fire resistance time [min]	220	206	> 250	> 250	> 250	224

† $k_2 = 2.0$, ‡ Au 50

Table 3 Simply supported beam B_1 with overhangs [26]. Comparisons between predicted and measured values at $t = 200$ min.

In case $\boldsymbol{A}$, when the contributions of $D_{cr,c}$, $D_{tr,c}$ and $D_{cr,s}$ are neglected in the numerical analysis, our results for the deflection w^* (see Fig. 2 for the definition of the deflection and the related cross-section) well agree up to about $t = 150$ min (see Fig. 8). At $t = 200$ min the measured deflection in B_{1a} is $w^*_{exp} = 12.4$ cm and $w^*_{exp} = 14.6$ cm in B_{1b}, while the finite-element analysis gives $w^* = 8.31$ cm, which is a lot less than the measured one. The related calculated horizontal displacement in the left outermost point of the beam, u^*, see Fig. 2 for the precise definition of the displacement, agrees well with the measured one up to time $t = 180$ min (Fig. 9). Later on, at $t = 200$ min, the differences are somewhat bigger: values, given by experiments B_{1a} and B_{1b}, are $u^*_{exp} = 6.2$ cm and 7.5 cm, respectively, compared to $u^* = 5.16$ cm, obtained in the calculation.

In case $\boldsymbol{B}$, the contribution of $D_{cr,c}$ is considered, but not that of $D_{tr,c}$ and $D_{cr,s}$. The result is that w^* increased somewhat (see Fig. 8), yet the error still grows with time. At $t = 200$ min, the deflection is $w^* = 8.66$ cm and the horizontal displacement is $u^* = 5.12$ cm. The fire resistant time is greater than 250 min. This indicates that the creep of concrete is not essential for the loss of stability of the simply supported beam in fire.

In case $\boldsymbol{C}$, the contributions of both $D_{cr,c}$ and $D_{tr,c}$ are considered and the contribution of $D_{cr,s}$ neglected. The resulting deflections again increase, while the horizontal displacement u^* decreases. At $t = 200$ min, the deflection is $w^* = 10.11$ cm and the horizontal displacement is $u^* = 5.02$ cm. The fire resistant time is still greater than 250 min.

The analysis of case $\boldsymbol{D}$ considers all kinds of the strain contributions. It clearly shows a decisive

effect of the viscosity of steel at temperatures above 400°C. Williams-Leir [41] provided the data for steel with a different creep characteristics. If we consider the steel with a mild creep characteristics (steel Austen 50), the agreement between measured and predicted response curves is sufficient (see Figs. 8 and 9). At $t = 200\,\text{min}$ the calculated displacements are $w^* = 12.41\,\text{cm}$ and $u^* = 5.28\,\text{cm}$. It is obvious that the creep of steel accelerates the collapse of the simply supported beam—the numerically obtained fire resistance time is now 223 min and the related collapse temperature is 1098°C.

The results show that w^* increases during fire and that u^* does so only if the creep in steel is considered (Fig. 9). The shape of the calculated $u^*(t)$ curve is similar to the measured ones. Observe a big difference between the measured and the predicted values of u^* at the start of the thermal load. Our guess is that this is due to the misinterpretation of the experimental results [26], see also the numerical results in [7, 17, 26].

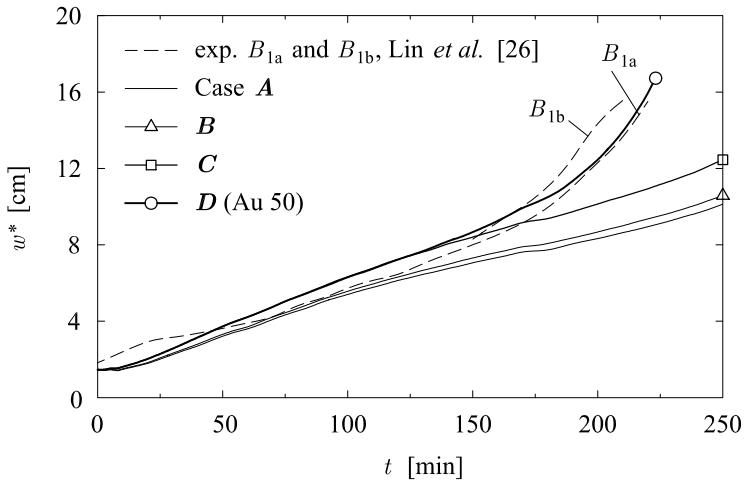

Fig. 8 Simply supported beam B_1 with overhangs [26]. Comparison of the variation of the predicted and measured vertical deflection w^* with time.

Fig. 10 shows the isolines of temperature, various strain components and stress at $t = 200\,\text{min}$ over the cross-section at which w^* is measured.

Stress–strain state in beam B_3. Beam B_3 differs with respect to beam B_1 in that B_3 has a much thicker concrete cover (57 mm compared to 38 mm in B_1). Material parameters are as in beam B_1, except for the elastic modulus at room temperature, which here takes the value $E_{c0} = 3\,050\,\text{kN/cm}^2$, and the strength of concrete, which is $f_{c0} = 2.96\,\text{kN/cm}^2$. In the analysis we considered all strain contributions. Some comparisons are displayed in Table 4.

This time the viscous parameters of steel with medium creep characteristics (A 149) appear to give better agreement for the vertical deflection than those of Austen 50, see Fig. 11. There, the response curve for case ***A*** (where $D_{\text{cr,c}}$, $D_{\text{tr,c}}$ and $D_{\text{cr,s}}$ are neglected) is depicted, too, again indicating that the contribution of steel creep strain to the response is essential.

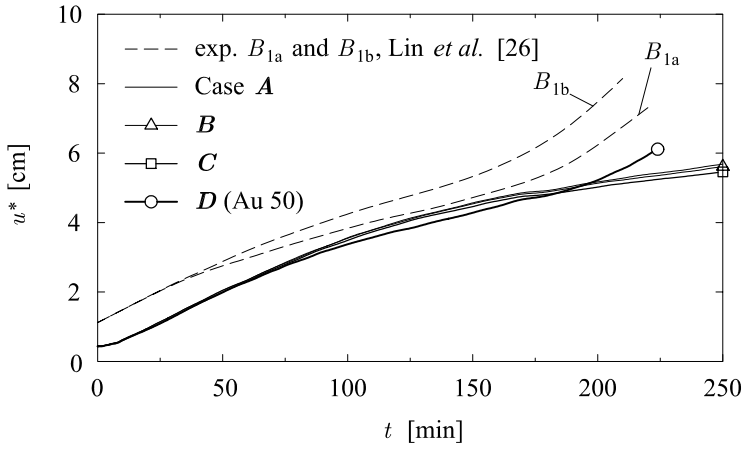

Fig. 9 Simply supported beam B_1 with overhangs [26]. Comparison of the variation of the predicted and measured horizontal displacement u^* at the left outermost point of beam with time.

	experiment [26]	finite element method		
	B_3	Case ***A***	Case ***D****	Cai *et al.* [7]
w^* [cm]	10.1	7.15	10.32	11.41
u^* [cm]	5.3	4.62	4.50	/
fire resistance time [min]	243	> 250	248	230

$^*k_2 = 2.0$ and A 149

Table 4 Simply supported beam B_3 with overhangs [26]. Comparisons between predicted and measured values at $t = 200\,\text{min}$.

A considerable disagreement can be observed between the numerical and the measured results for u^* (Fig. 12). Again an unexpected difference is observed at the onset of the fire already, which then remains roughly the same during fire. At $t = 200\,\text{min}$ the displacement u^* takes the value $4.55\,\text{cm}$, if viscosity of steel A 149 is considered, compared to $u^*_{\text{exp}} = 5.3\,\text{cm}$ obtained experimentally [26].

The fire resistance time of beam B_3 with a thicker concrete cover proves to be higher than that of beam B_1, although, due to a smaller static height of the cross-section B_3, it has a considerably smaller bearing capacity at room temperature. The difference between the resistance times is about 11 %: 248 min compared to 223 min for the B_3 and B_1 beams, respectively. The critical deflection at the collapse of beam B_3 is $w^* = 17.6\,\text{cm}$, which is about 3.7 % more than 16.7 cm found in beam B_1.

Stress–strain state in beam B_5. Beam B_5 is characterised by having a cooling phase after the peak temperature takes place, which is a good model of a realistic fire scenario. The SDHI-M fire curve is assumed. The geometrical data remains as in beam B_1 (see Fig. 2). Elastic modulus of concrete was assumed to be $E_{\text{cm0}} = 3\,150\,\text{kN/cm}^2$, while the strength of concrete was $f_{\text{c0}} = 3.37\,\text{kN/cm}^2$. The

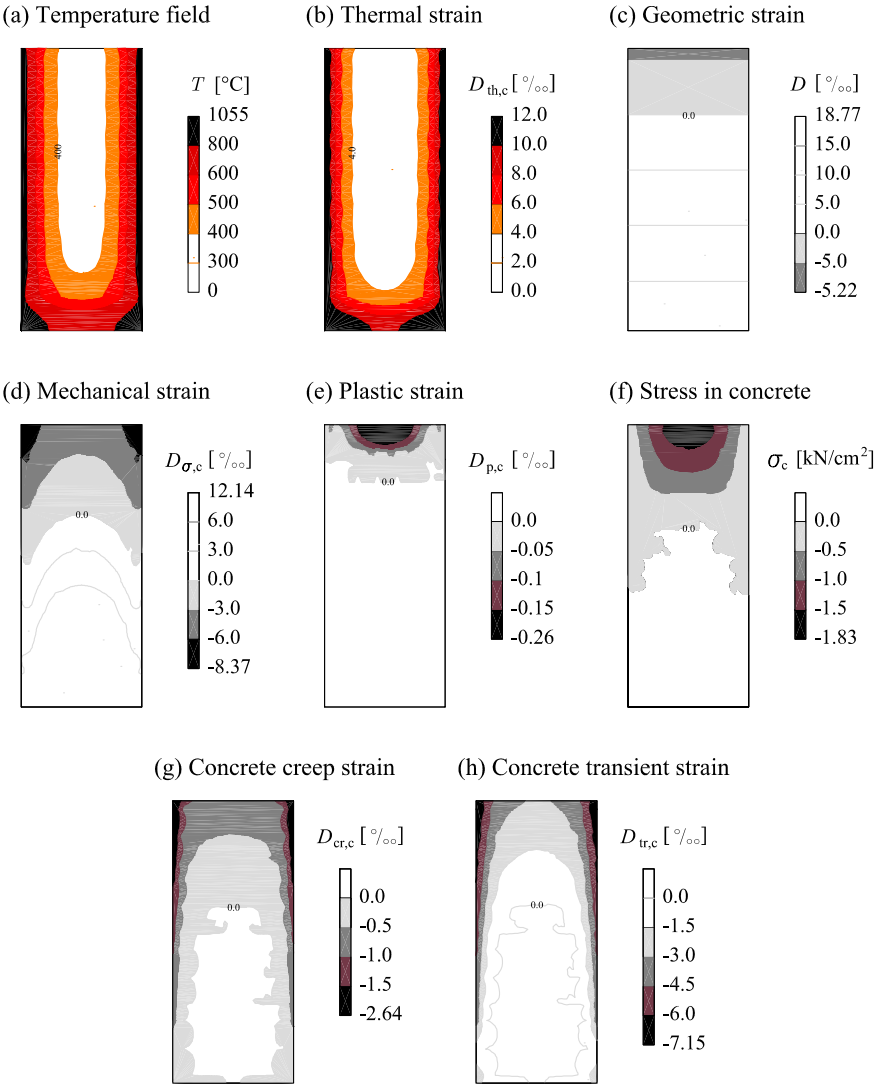

Fig. 10 Simply supported beam B_1 with overhangs [26]. Temperature field, thermal strain, geometric (total) strain, mechanical strain, plastic strain, stress, creep and transient strains in the concrete cross-section of w^* at $t = 200\,\text{min}$.

remaining material parameters were as in beam B_1.

Figs. 13 and 14 show the displacement–time curves. The numerical results of cases ***A***–***D*** along with the experimental results of [26] and the numerical results given in [7] are shown. We see that the contributions of creep strain in steel are minor, which is due to a relatively low temperature, about 400°C, reached in the reinforcement. The creep in concrete and the transient strain somewhat increase the deflections. The resistance time of the simply supported beam is not affected by various strain contributions. Notice also a very good correspondence between our numerical results marked ***D*** (Au 50) and the results in [7] in a later stages of fire ($t > 100\,\text{min}$).

In contrast to the ASTM fire loads, where the deflection increased all the time, in the SDHI-M

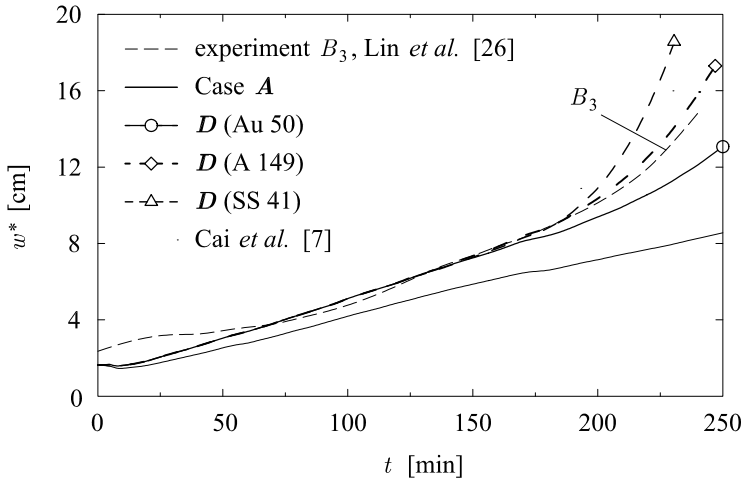

Fig. 11 Simply supported beam B_3 with overhangs [26]. Variation of w^* with time.

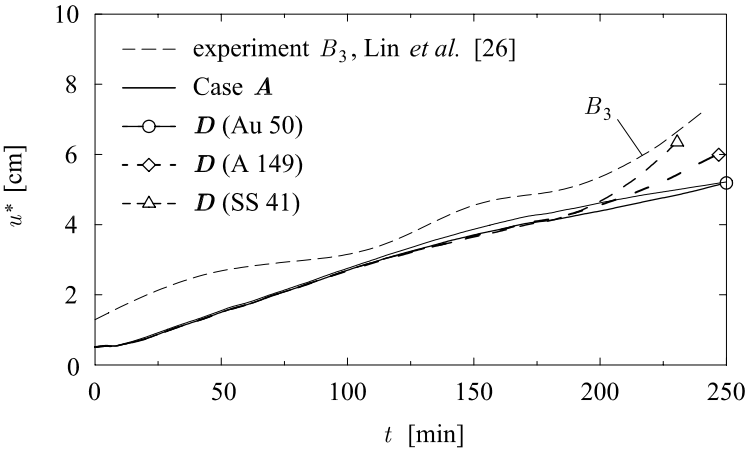

Fig. 12 Simply supported beam B_3 with overhangs [26]. Variation of u^* with time.

fire, the deflection (as well as the horizontal displacement) starts decreasing after it reaches its peak value $w^*_{\rm cr} = 5.60\,$cm (Fig. 13) at $t_{\rm cr} = 110\,$min. The related horizontal displacement is $u^*_{\rm cr} = 3.12\,$cm. The corresponding measured values were $w^*_{\rm exp} = 7.4\,$cm at 120 min and $u^*_{\rm exp} = 4.4\,$cm at 105 min.

It is apparent that the SDHI-M fire load is much less critical than the ASTM one. The beam safely standed the fire. The maximal calculated deflection was about 6 cm, which is less than 40 % of that in the ASTM fire at the collapse at 223 min.

Fig. 15 shows the isolines of temperature, various strain components and stress at $t = 200\,$min in the cross-section of w^*.

3.2 Clamped reinforced concrete column

In this example we compare the results of our numerical model with the experimental results of

	experiment [26]	finite element method		
extreme values	B_5	Case $\boldsymbol{A}$	Case $\boldsymbol{D}^*$	Cai *et al.* [7]
w^* [cm]	7.4	4.76	5.60	5.93
w^*–critical time [min]	120	105	110	90
u^* [cm]	4.4	3.22	3.12	/
u^*–critical time [min]	105	105	105	/

$^*k_2 = 2.0$ and Au50

Table 5 Simply supported beam B_5 with overhangs [26]. Comparisons between extreme predicted and measured values.

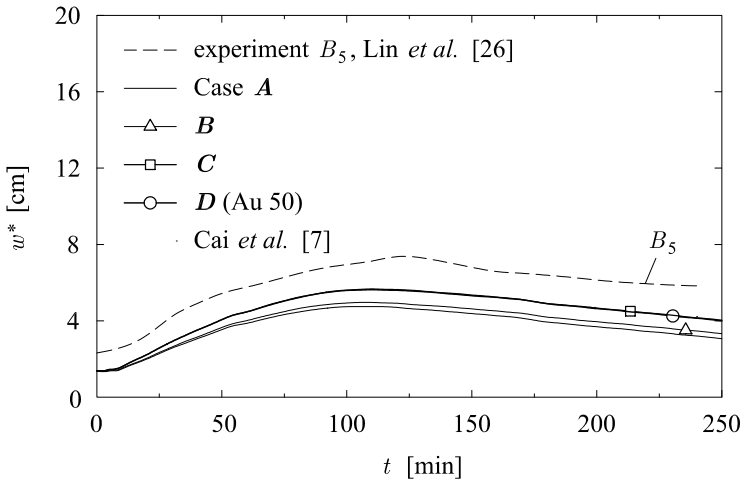

Fig. 13 Simply supported beam B_5 with overhangs [26]. Variation of w^* with time.

full-scale laboratory fire tests on the centrically loaded reinforced concrete column. The tests were performed by Kodur *et al.* [23]. No explosive spalling was detected during fire in their experiment. The geometric and loading data are given in Fig. 16. The self weight of the column is considered as an axial traction. In order to simulate a fire situation in a laboratory, a column was exposed to hot surrounding air in such a way that the air temperature (generated by the furnace) was changing according to the ASTM fire curve [2]. The measured fire resistance time of the column was 278 min [23]. The related critical temperature was 1137°C. The remaining material parameters and their temperature dependence, needed in the numerical analysis of the mechanical response, were estimated using the given strengths and the data from Eurocode 2 [10].

3.2.1 Temperature distribution in the column

Thermal parameters, such as the conductivity k_c, the convection heat transfer coefficient h_c and

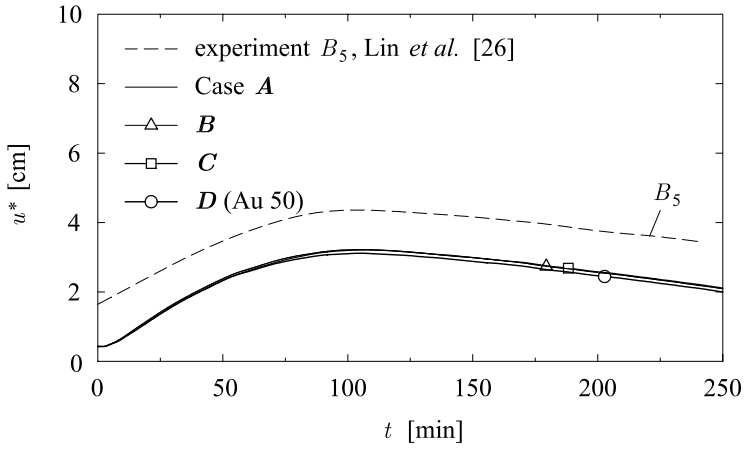

Fig. 14 Simply supported beam B_5 with overhangs [26]. Variation of u^* with time.

the emissivity ε_{r}, were not presented in the report by Kodur *et al.* [23] and were hence here selected in such a manner that the numerically predicted and the measured temperatures in concrete agreed as much as possible ($\varepsilon_{\mathrm{r}} = 0.3$, $h_{\mathrm{c}} = 20\,\mathrm{W/mK}$, the graph of k_{c} is depicted in Fig. 17). End parts of the column were not exposed to fire (temperature was held at $T = 20°\mathrm{C}$), so that the actual length of the column exposed to fire was 310 cm. Fig. 18 shows the calculated and the measured temperature distributions at various depths along the center-line in the concrete cross-section. We see that somewhat artificially selected thermal parameters this time resulted in a good agreement between the numerically predicted and the measured temperatures. The calculated time-dependent temperature field over the cross-section was used as the thermal load of the column in the subsequent mechanical analysis.

3.2.2 Stress–strain state of the column

In order to determine the mechanical response of the column subjected to thermal and mechanical loads, the column was modelled by six beam finite elements, in which axial and bending deformations were interpolated with the Lagrangian polynomials of the fourth order. To initiate buckling, the axis of the column was made imperfect with small eccentricity 0.01 cm. For the integration of the stresses over the cross-section, a total of 180 integration points for a half of the cross-section was used. The thermo-mechanical properties of concrete with siliceous aggregate and cold worked reinforcing steel were used.

Fig. 19 shows how the measured axial displacement was changing with time. We can see that the axial displacement was increasing during the first 180 min. This corresponds to the elongation of the column which is due to the growing temperature and its related thermal strain. Subsequently, the axial displacement started decreasing. At some instant of time this caused the shortening of the column, which was due to the rapid increase of creep and transient strains. This kind of behaviour is typical for reinforced concrete columns.

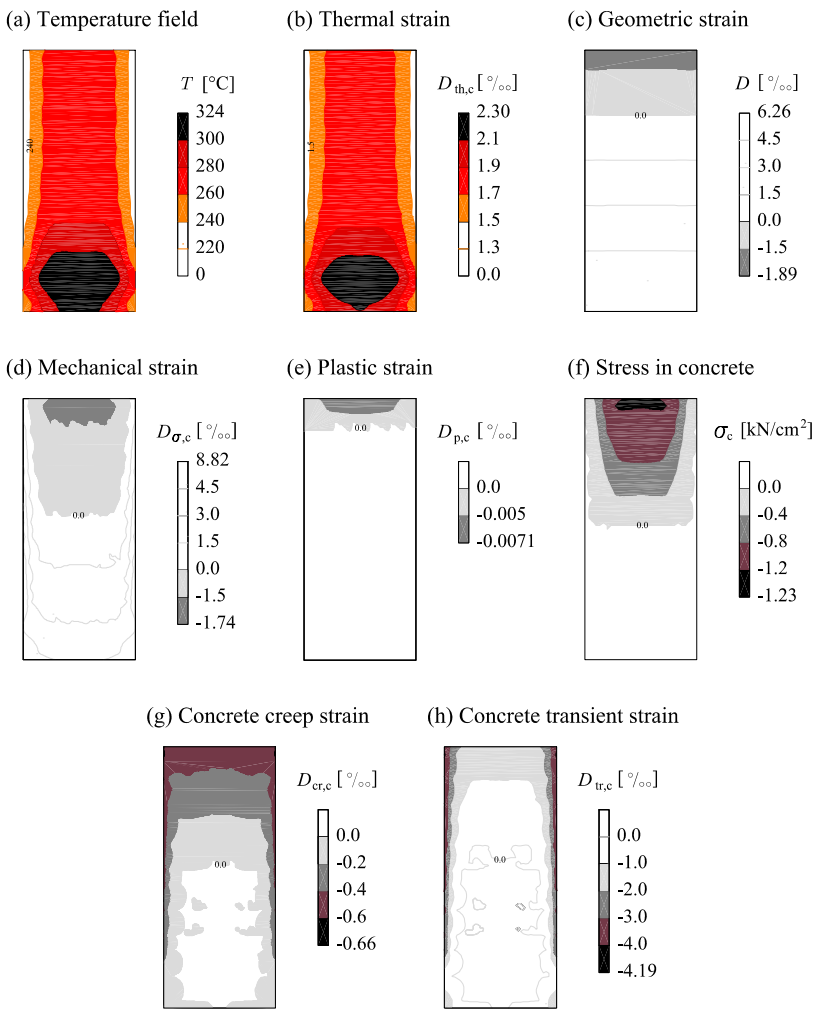

Fig. 15 Simply supported beam B_5 with overhangs [26]. Temperature field, thermal strain, geometric strain, mechanical strain, plastic strain, stress, creep and transient strains in the concrete cross-section of w^* at $t = 200\,\text{min}$.

We find it interesting to study the effect of individual strain parts in concrete and steel on the mechanical behaviour of the column. In case $\boldsymbol{A}$, when only the thermal strain (D_{th}) is considered, the axial displacement u^* of the column becomes maximal at about 110 min and is much greater than the measured one (see Fig. 19). This remains true in case $\boldsymbol{B}$, too, when the creep strain of concrete ($D_{\text{cr,c}}$) is also considered. The calculated axial displacement at the collapse at about 279 min is this time notably smaller than the measured one. In case $\boldsymbol{C}$, when the transient strain of concrete ($D_{\text{tr,c}}$) is additionally considered, the displacement changed considerably, although we used the least recommended value (1.8) for the constant k_2 in the transient strain increment expression

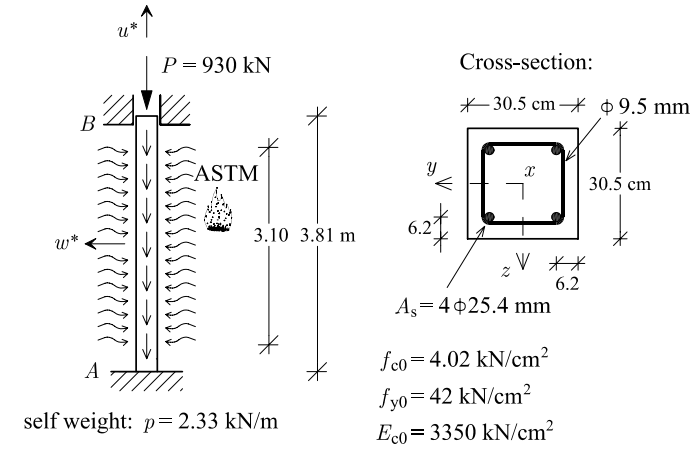

Fig. 16 Clamped centrically loaded reinforced concrete column in fire [23].

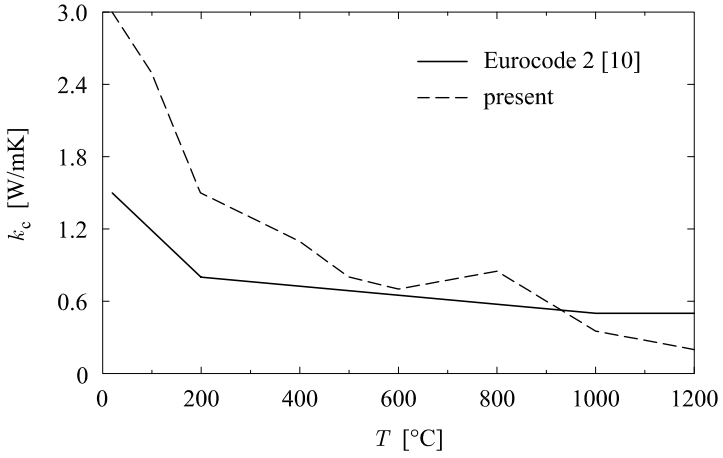

Fig. 17 Clamped centrically loaded reinforced concrete column in fire [23]. The variation of conductivity k_c with temperature.

($u^*_{cr} = 2.45\,\text{cm}$, $u^*_{cr,exp} = 2.25\,\text{cm}$). The creep strain in steel ($D_{cr,s}$) – case ***D*** – does not effect the axial displacement considerably, because the highest temperature in reinforcing steel is only about 400°C (see Fig. 18) and because steel Au 50 which is the least sensitive to creep was used.

Surprisingly, the calculated fire resistance time does not depend much on which strain parts are considered or neglected and rather well equals to the resistance time measured in experiment. Fig. 19 also shows the variation with time of the calculated lateral displacement w^* at the mid-point of the column. A sudden increase in w^* indicates the onset of buckling of the column at time 255 min and the subsequent critical state at about 284 min (which corresponds to fire temperature 1140°C), which is close to 278 min reported in Kodur *et al.* [23]. The essential numerical values are displayed in Table 6.

The results of the numerical analysis make it possible to assess the contribution of individual

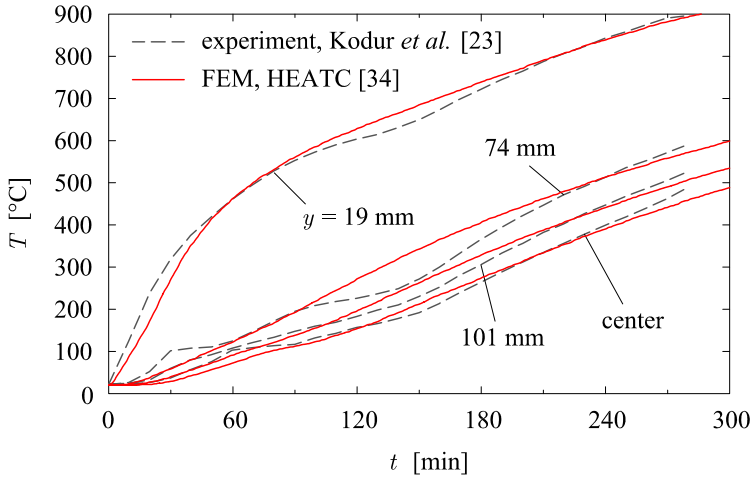

Fig. 18 Clamped centrically loaded reinforced concrete column in fire [23]. The comparison between the measured and the predicted temperature distributions at various depths along the center-line in concrete cross-section.

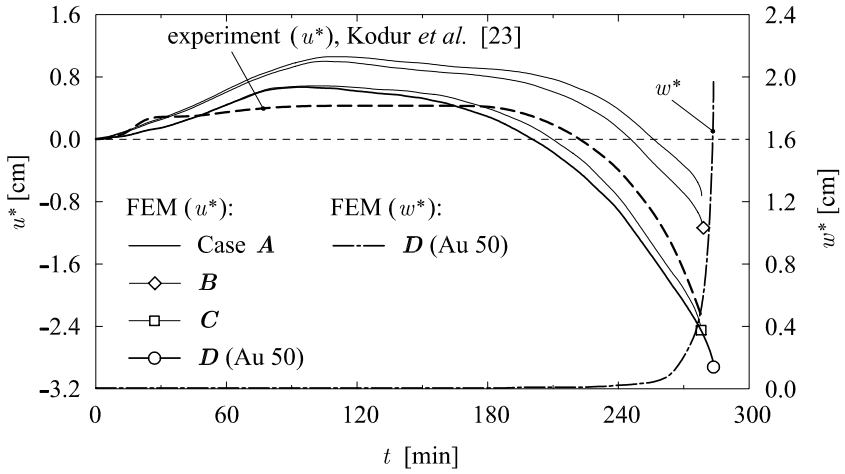

Fig. 19 Clamped centrically loaded reinforced concrete column in fire [23]. The variation of axial displacement (u^*) at point B and the lateral displacement at the mid-point of the column (w^*) with time.

strain parts to the integral response of the column. Fig. 20 shows the isolines of thermal, geometric, mechanical, creep and transient strains and stress at the mid-point of the concrete cross-section at 250 min. At this instant the column is a little buckled; that is why the geometrical strain is not homogeneous across the section. The remaining strains vary over the cross-section. With the exception of the mechanical strain, the strains attain their maximal values at the surface of the cross-section. Note that the concrete transient strains are comparable in size with thermal or mechanical

	experiment [23]	present			
	TNC1	Case $\boldsymbol{A}$	Case $\boldsymbol{B}$	Case $\boldsymbol{C}^{\dagger}$	Case $\boldsymbol{D}^{\ddagger}$
u^* [cm]	-0.72	0.16	-0.12	-1.11	-1.27
w^* [cm]	/	0.02	0.02	0.03	0.03
fire resistance time [min]	278	278	279	278	284

† $k_2 = 1.8$

‡ Au 50

Table 6 Clamped centrically loaded reinforced concrete column in fire [23]. Comparisons between measured and predicted values at $t = 250\,\text{min}$.

strains. They are, however, compressive, in contrast to thermal strains which are tensile. Mechanical strains are also compressive; they are maximal at regions positionned a few centimetres away from the surface of the section. The stresses in concrete are not homogeneous over the section. They are maximal at the centre region of the section. Fig. 20d shows that about one third of the section experiences only a very low stress (between 0 and $-0.5\,\text{kN/cm}^2$) at this instant. It is instructive to quantify particular strain contributions to the total strain at material point placed at the uppermost right corner of the cross-section ($y = 14.91$ cm, $z = -14.39$ cm): thermal strain $D_{\text{th,c}} = 14$ °/₀₀, mechanical strain $D_{\sigma,c} = -8.02$ °/₀₀, creep strain $D_{\text{cr},c} = -3.01$ °/₀₀, transient strain $D_{tr,c} = -7.51$ °/₀₀, total strain $D = -4.54$ °/₀₀.

4 Conclusions

Modelling the behaviour of reinforced concrete frame structures in fire is a difficult task. In this paper we employ a two-step solution strategy and introduce a number of further simplifications in order to make the analysis practically feasible. The first step consists of determining the temperature distribution over the structure at each time during fire, which is, in the second step, used as the thermal load. The frame structure is modelled by strain-based, kinematically exact beam finite elements introduced previously in [4]. A number of assumptions have to be introduced concerning the constitutive laws of materials at elevated temperature and several guesses for values of their thermal and material parameters have to be made due to the lack of sufficiently documented and statistically reliable experimental data. The numerically predicted results for two simple reinforced concrete structures subject to fire with or without a cooling phase have been confronted with the experimental data and promising results have been obtained. The comparisons of the results are described in the body of the paper in full detail. The following further short conclusions and indications can be given:

- The agreement of the fire resistance times and critical deflections between the predicted and the experimental values was found satisfactory. A much less agreement was found regarding

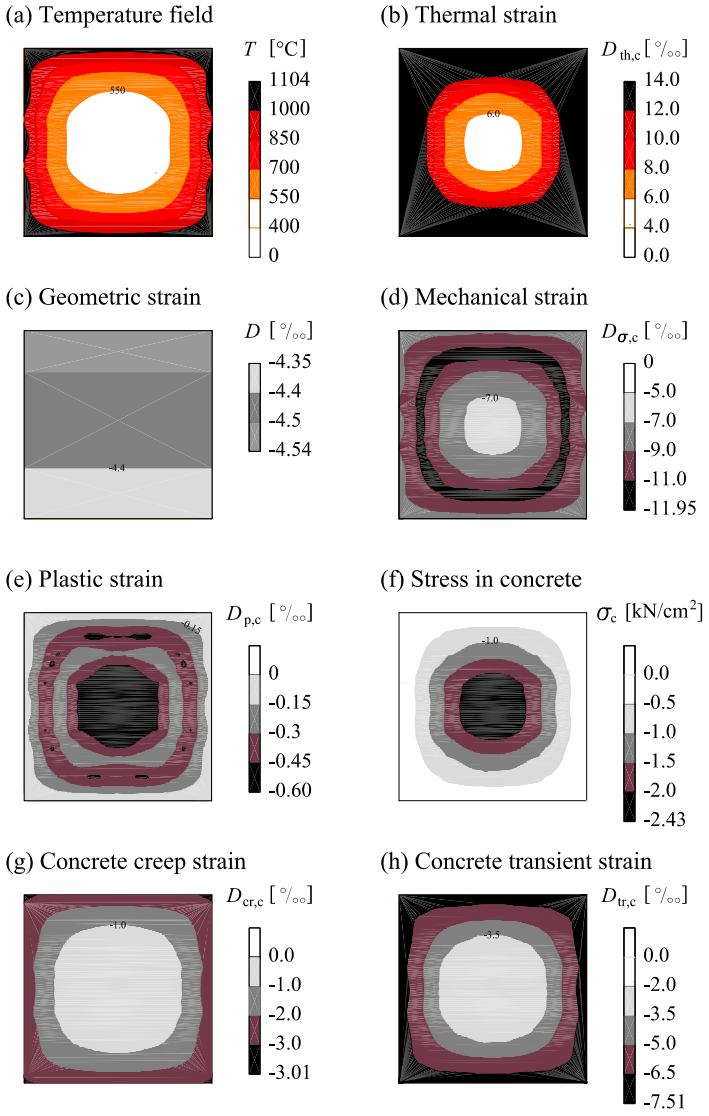

Fig. 20 Clamped centrically loaded reinforced concrete column in fire [23]. Isolines for various strains and stress in concrete at mid-point cross-section at $t = 250\,\text{min}$.

the time and space distributions of temperature over the beam cross-sections. Thus, our model to predict the temperature distributions in concrete during fire needs much to be improved.

- The study of the contributions of particular strains to the overall response of a structure shows that the fire resistance time is not effected by creep and transient strains in concrete if the structure is simple enough. This is in keeping with the building standard Eurocode 2.

- By contrast, the creep in steel reinforcement becomes crucial as soon as temperature in reinforcement bars exceeds 400°C. The ability of the prediction of the fire resistance hence becomes largely dependent on the quantitative values of viscous parameters of steel. Commercial steels used for reinforcing should therefore obligatory have the creep specifications at elevated tem-

peratures indicating the suitability of steel bars for use in potentially fire-exposed concrete structures.

References

[1] Anderberg Y, Thelandersson S. Stress and deformation characteristics of concrete at high temperatures, 2. Experimental investigation and material behaviour model. Lund Institute of Technology, Sweden, 1976.

[2] ASTM E-119-76: Standard Methods of Fire Tests of Building Construction and Materials. Annual book of ASTM standards, Part 18, American Society for Testing and Materials, 1976.

[3] Bažant ZP, Kaplan MF. Concrete at high temperatures. Longman Group Limited, 1996.

[4] Bratina S, Čas B, Saje M, Planinc I. Numerical modelling of behaviour of reinforced concrete columns in fire and comparison with Eurocode 2. International Journal of Solids and Structures, 2005;42(21-22):5715–33.

[5] Bratina S, Saje M, Planinc I. On materially and geometrically non-linear analysis of reinforced concrete planar frames. International Journal of Solids and Structures 2004;41:7181–7207.

[6] Bratina S, Planinc I, Saje M, Turk G. Non-linear fire-resistance analysis of reinforced concrete beams. Structural Engineering and Mechanics 2003;16(6):695–712.

[7] Cai J, Burgess I, Plank R. A generalised steel/reinforced concrete beam-column element model for fire conditions. Engineering Structures 2003;25:817–33.

[8] Cruz CR. Elastic properties of concrete at high temperatures. Journal of the PCA Research and Development Laboratories 1966;8:37–45.

[9] Cruz CR. Apparatus for measuring creep of concrete at high temperatures. Journal of the PCA Research and Development Laboratories 1968;10(3):36–42.

[10] Eurocode 2: Design of Concrete Structures, Part 1-2: General Rules—Structural Fire Design. prEN 1992-1-2, 2002.

[11] Gamal NA, Hurst JP. Coupled heat and mass transport phenomena in siliceous aggregate concrete slabs subjected to fire. Fire and Materials 1997;21:161–8.

[12] Gawin D, Pesavento F, Schrefler BA. Modelling of hygro-thermal behaviour and damage of concrete at temperature above the critical point of water. International Journal for Numerical and Analytical Methods in Geomechanics 2002;26:537–62.

[13] Gawin D, Pesavento F, Schrefler BA. Modelling of hygro-thermal behaviour and damage of concrete at temperature with thermo-chemical and mechanical material degradation. Computer Methods in Applied Mechanics and Engineering 2003;192:1731–71.

[14] Harmathy TZ. Fire Safety Design and Concrete. London: Longman, 1993.

[15] Hertz KD. Limits of spalling of fire-exposed concrete. Fire Safety Journal 2003;38:103–16.

[16] Huang Z, Platten A. Nonlinear finite element analysis of planar reinforced concrete members subjected to fires. ACI Structural Journal 1997;94(3):272-82.

[17] Huang Z, Platten A, Roberts J. Non-linear finite element model to predict temperature histories within reinforced concrete in fire. Building and Environment 1996;31(2):109–53.

[18] Ichikawa Y, England GL. Prediction of moisture migration and pore pressure build-up in concrete at high temperatures. Nuclear Engineering and Design 2004;228:245–59.

[19] Kalifa P, Menneteau F-D, Quenard D. Spalling and pore pressure in HPC at high temperatures. Cement and Concrete Research 2000;30:1915–27.

[20] Kang SW, Hong SG. Behaviour of concrete with thermal creep at elevated temperatures. Third International Conference on Concrete under Severe Conditions, CONSEC'01, Vancouver, 2001.

[21] Khennane A, Baker G. Uniaxial model for concrete under variable temperature and stress. Journal of Engineering Mechanics 1993;119(8):1507–25.

[22] Khoury GA, Majorana CE, Pesavento F, Schrefler BA. Modelling of heated concrete. Magazine of Concrete Research 2002;54(2):77–101.

[23] Kodur WKR, Cheng F-P, Wang T-C, Sultan MA. Effect of strength and fiber reinforcement on fire resistance of high-strength concrete columns. Journal of Structural Engineering 2003;129(2):253–9.

[24] Lie TT, Irwin RJ. Method to calculate the fire resistance of reinforced concrete columns with rectangular cross section. ACI Structural Journal 1993;90(1):52–60.

[25] Li LY, Purkiss J. Stress–strain constitutive equations of concrete material at elevated temperatures. Fire Safety Journal 2005;40:669–86.

[26] Lin TD, Ellingwood B, Piet O. Flexural and shear behaviour of reinforced concrete beams during fire tests. PCA, Research and Development Bulletin, Report No. NBS-GCR-87-536, Center for Fire Resarch, National Bureau of Standards, Washington, 1988.

[27] Lien HP, Wittmann FH. Coupled heat and mass transfer in concrete elements at elevated temperatures. Nuclear Engineering and Design 1995;156:109–19.

[28] Luccioni BM, Figueroa MI, Danesi RF. Thermo-mechanic model for concrete exposed to elevated temperatures. Engineering Structures 2003;25:729–42.

[29] Nechnech W, Meftah F, Reynouard JM. An elasto-plastic damage model for plain concrete subjected to high temperatures. Engineering Structures 2002;24:597–611.

[30] Planinc I, Saje M, Čas B. On the local stability condition in the planar beam finite element. Structural Engineering and Mechanics 2001;12:507–26.

[31] Purkiss JA. Fire Safety Engineering Design of Structures. Butterworth-Heinemann, 1996.

[32] Rilem TC 129-MHT: Test Methods for Mechanical Properties of Concrete at High Temperatures, Recommendations: Part 7: Transient Creep for service and accident conditions. Material and Structures 1998;31:290–5.

[33] Saje M, Planinc I, Bratina S. Large displacement and instability of beam-like structural system. NATO Advanced Research Workshop 2004;329–50.

[34] Saje M, Turk G. HEATC. Computer programme for nonlinear transient heat conduction problems. University of Ljubljana, Faculty of Civil and Geodetic Engineering, 1987 [in Slovene].

[35] Schneider U. Properties of Materials at High Temperatures – Concrete. 2nd edn, RILEM Report, Gesamthochschule Kassel, Germany.

[36] Schneider U. Concrete at high temperatures – A general review. Fire Safety Journal 1988;13:55-68.

[37] Tenchev RT, Li LY, Purkiss JA. Finite element analysis of coupled heat and moisture transfer in concrete subjected to fire. Numerical Heat Transfer, Part A 2001;39:685–710.

[38] Tenchev RT, Purnell P. An application of a damage constitutive model to concrete at high temperature and prediction of spalling. International Journal of Solids and Structures 2005;42:6550–65.

[39] Ulm FJ, Coussy O, Bažant ZP. The 'Chunnel' fire. I: Chemoplastic softening in rapidly heated concrete. Journal of Engineering Mechanics ASCE 1999; 125(3):272–82.

[40] Ulm FJ, Acker P, Lévy M. The 'Chunnel' fire. II: Analysis of concrete damage. Journal of Engineering Mechanics ASCE 1999; 125(3):283–89.

[41] Williams-Leir G. Creep of structural steel in fire: Analytical expressions. Fire and Materials 1983;7(2):73–8.

[42] Zha XX. Three-dimensional non-linear analysis of reinforced concrete members in fire. Building and Environment 2003;38:297–307.